

Article

Molecular Dynamics Study of Anti-Wear Erosion and Corrosion Protection of PTFE/Al₂O₃ (010) Coating Composite in Water Hydraulic Valves

Masoud Kamoleka Mlela , He Xu * and Haihang Wang 

College of Mechanical and Electrical Engineering, Harbin Engineering University, Harbin 150001, China; masoudkamoleka@gmail.com or mkamoleka@mustnet.ac.tz (M.K.M.); wanghaihang@hrbeu.edu.cn (H.W.)

* Correspondence: xuhe@hrbeu.edu.cn; Tel.: +86-133-5111-7608

Received: 6 November 2020; Accepted: 10 December 2020; Published: 12 December 2020



Abstract: Cavitation erosion and corrosion commonly occur on the surface of fluid dynamic system components, mostly water hydraulic valves, causing the failure of metal parts. Coating of polytetrafluoroethylene (PTFE) on Al₂O₃ (010) was created by varying the chain length of polytetrafluoroethylene. Calculations were conducted by molecular dynamic (MD) simulations. This study shows that the K10 and K20 chain lengths' mechanical properties possess negative elastic, shear, and bulk modulus values. We have found that the K10 chain length composition shows the high results of binding energy and negative bulk modulus of 6267.16 kJ/mol and −3709.54 GPa, respectively. The K10 chain length was observed to possess a higher cohesive energy density (CED) and solubility parameter of $(6.885 \pm 0.00076) \times 10^9$ J/m³ and (82.974 ± 0.005) (J/cm³)^{0.5}, respectively. It was also found that increasing the chain length contributes to decreasing the binding energy and solubility parameter of PTFE/Al₂O₃ (010) composition. These results are vital for overcoming the repetitive regime of high compressive strength of water microjets on the valves' material surface. Improved values of the cohesive energy density and solubility parameters imply the water's superior hydrophobic effect.

Keywords: polymer; molecular dynamics simulation; mechanical properties; binding energy; cavitation erosion; surface corrosion; surface hydrophobicity; solubility parameters; water hydraulics' valves

1. Introduction

Polymeric materials are prevalent in nature and daily life. It has been demonstrated that composite materials with polymer matrices cover surfaces pressured with cavitation flows and abrasive pattern suspension [1]. Polymers are most widely used in applications and structures that work under such hydrodynamic fluid conditions due to the characteristics of mechanical resilience, chemical degradation, and abrasive erosion resistance. Protecting the surfaces of hydro mechanical parts that work under cavitation wear conditions, such as rotors and valves in hydraulic machines, is among such applications [1]. Molecular dynamic simulations have contributed a lot in recent years to amorphous alloy development and improvement. Several investigations have been documented into amorphous alloy forming capacity and mechanical properties using molecular dynamic simulations [2]. Xu et al. [3] uses Monte Carlo dynamic simulations to investigate the chain length effects in polymer compound systems of specific chain length on stereocomplex crystallites (SCs). Studies have shown that decreasing the chain's length increases the concluding stereocomplex crystallites material. In the short-chain systems, three aspects lead to improved SC creation, comprising miscibility between dissimilar polymer types, chain flexibility, and nuclear mode. The structures with shorter chains are

more miscible, have better compartment mobility, and tend to crystallize in a parallel intermolecular alignment; thus, providing a more significant SC material than long chains.

Meanwhile, in ref. [4], Chen et al. conducted a study investigating the influence of glucose polymer chain length on the heat and physical characteristics of milk-protein isolate (MPI) sugar-nutrient drinks containing 8.5% *w/w* total protein and 5% *w/w* carbohydrate. The findings show that the chain length of the glucose polymer heavily influences MPI carbohydrate supplement beverages. Zhao et al. [5] also investigated chain-length and temperature-based tensile and shear failure activity using molecular dynamic simulations in amorphous polymers. They concluded that the breakup intensity under shear and tension rises with chain length and the temperature increases. The breakup rates under shear are often higher for a defined chain length and temperature than those below the same high strain. The tensile and shear stresses decrease with rising temperature for a given chain length. The effects of polymer chain length on formless drug recrystallization hindrance were investigated by Pacult et al. [6].

To contemplate this issue, they arranged a drug–polymer mix in the proportion of 10:1 (drug to polymer) comprising bicalutamide (BIC) and polyvinylpyrrolidone (PVP) with peculiar chain lengths K10, K30, K90. They believe that the polymer chain may have different configurations in space that contribute to better or worse stability in research, based on its length. Mlela et al. [7] aimed to match Cr₂O₃, Al₂O₃, and Ti₂O₃ with the most appropriate polymer coating. Through using the Preference Ranking Organization Method for Enrichment Evaluations (PROMETHEE), the most robust obtained polymer in a watery environment valve with an evaluated efficiency attribute is polytetrafluoroethylene with a greater outranking (0.5932052). Their molecular dynamics studied the robust bonding concerning the superior cleave plane between polytetrafluoroethylene and the selected substrate. PTFE/Al₂O₃ cleaved in (010) crystallographic plane was found to have the strongest bond in terms of binding energy (3188 kJ/mol).

In this paper, we carried out molecular dynamic (MD) simulations of PTFE/Al₂O₃ (010) by varying the PTFE chain length to calculate the binding energy, mechanical properties, cohesive energy density (CED), and solubility parameter. The greater the mechanical properties' parameters of PTFE/Al₂O₃ (010), the greater the potential to resist stress without microjet deformation and breakage. Binding energy and coherent energy density (CED) reflect their component molecules' bonding strength. The solubility parameter holds great promise for developing a poorly water-soluble composition and, hence, smaller corrosion vulnerability. This work's results significantly impact the protection of water hydraulics' valves from erosion and corrosion and thus improve the water hydraulic system's performance.

2. Method and Approach

Molecular Dynamics (MD) Simulation and Properties Calculation

By utilizing Material Studio[®] software version 7.0 created by Accelrys Inc. (San Diego, CA, USA), molecular dynamic simulations were applied to examine the binding energies, mechanical and dissolvability properties of the various PTFE/Al₂O₃ (010). Figure 1 shows the simulation and calculation models of different phases of this work. In this research, as seen in Figure 2a,b, tasks were to build the cleaved crystal surface of Al₂O₃ (010) of a thickness of 5.4539 nm, with the lattice parameters of $U = 1.2991$ nm, $V = 0.4759$ nm, and $\theta = 90^\circ$. The next task was to optimize the geometry using the Forcite module obtained in materials studio (MS) version 7.0 of Accelrys Inc. and a smart algorithm [8] with the maximum iteration of 1000 steps, with ultra-fine quality that employs 8.368×10^{-5} kJ/mol of convergence energy and a force tolerance of 0.04184 kJ/mol/nm with the displacement of 1.0×10^{-6} nm. The surface of the crystals of Al₂O₃ (010) was minimized further by the discover module using a smarter ultra-fine minimizer with the maximum iteration of 2000 to achieve the stable structure of the lowest energy.

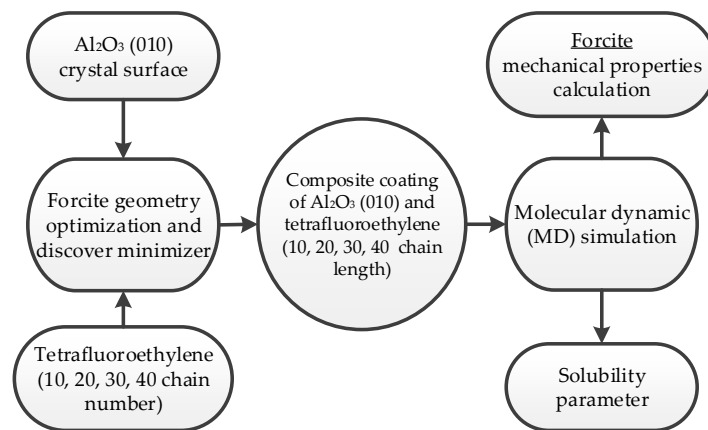


Figure 1. Molecular dynamics simulation and calculation models.

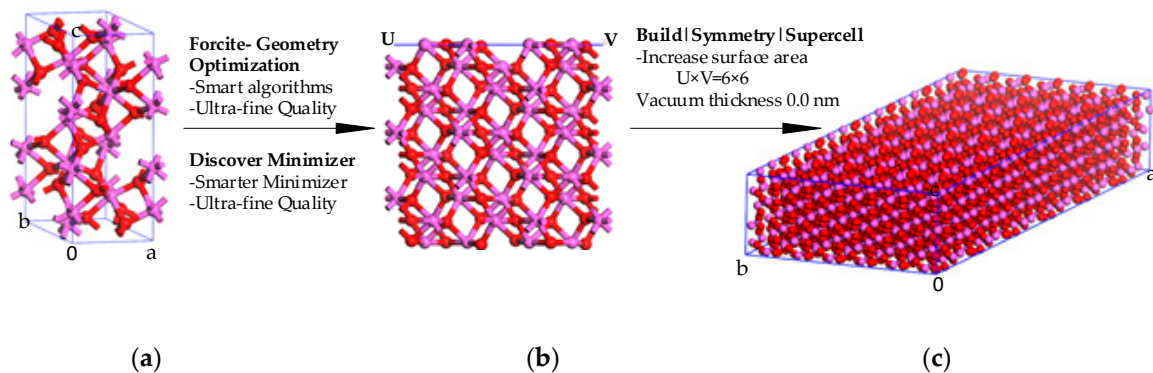


Figure 2. Cleave and relax the surface (0, a, b, c represent 3D-axis of hexagonal and triclinic lattices, and where U and V represent 2D-axis of oblique lattice) (a) 3D hexagonal, (b) 2D oblique, (c) 3D triclinic.

The Al_2O_3 (010) surface area was increased to obtain the 3D periodicity of the lattice vector of $U \times V = 6 \times 6$ by keeping a vacuum thickness of 0.0 nm. The 3D triclinic crystal lattice had the parameters of $a = 7.7946$ nm, $b = 2.8554$ nm, $c = 2.8554$ nm, and $\alpha = \beta = \gamma = 90^\circ$ was formed, see Figure 2c. The monomer repeat unit, tetrafluoroethylene, was imported from the materials library in the materials studio (MS) version 7.0 of Accelrys Inc. to build a polymer and amorphous cell. As usual, the job optimized by Forcite uses ultra-fine quality and a smart algorithm with the 1.0×10^3 maximum number of geometry optimization cycles (maximum iteration). By specifying the temperature 298 K, 2.20 g/cm^3 targeted density, the periodic amorphous cells of the final configuration were created in the amorphous cell tool, as Figure 3 shows. Table 1 gives the designated chain number, chain length, and polymer configuration of a different model. We must bring together the Al_2O_3 (010) surface layer and the other polytetrafluoroethylene layer for interaction. We specified a vacuum of 7.0 nm spacing for polytetrafluoroethylene in *c*-direction to secure enough space for physicochemical phenomena. The molecular dynamics simulation is essential for obtaining the actual density and conformation of wear-resistant coating to reach the equilibration state. We established the simulation at room temperature (298 K), with the Andersen temperature control system with a collision frequency of every 325 steps. The velocity Verlet integrator algorithm was employed considering the canonical ensemble of the constant number of particles, constant volume, and constant temperature (i.e., NVT)

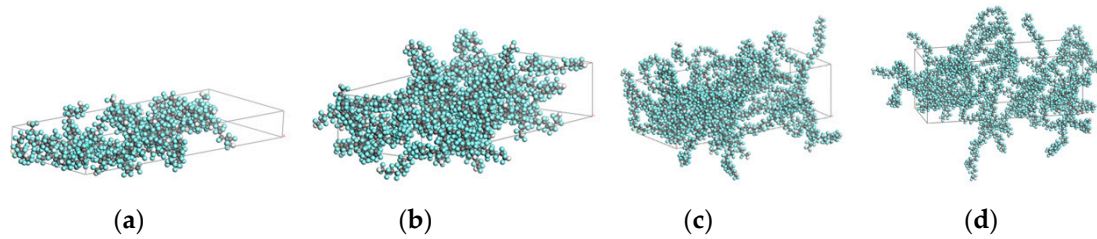


Figure 3. Amorphous cell of polytetrafluoroethylene. (a) K10 chain length with c parameter of 0.747 nm, (b) K20 chain length with c parameter of 1.493 nm, (c) K30 chain length with c parameter of 2.240 nm, (d) K40 chain length with c parameter of 2.985 nm.

Table 1. The designated number of chains, chain length, and polymer configuration of a different model.

Chain Length (K)	Number of Chains	Number of Configuration	Amorphous Cell Parameter (nm)
10	10	2	$a = 7.795, b = 2.855,$ $c = 0.747$
20	10	2	$a = 7.795, b = 2.855,$ $c = 1.493$
30	10	2	$a = 7.795, b = 2.855,$ $c = 2.239$
40	10	2	$a = 7.795, b = 2.855,$ $c = 2.985$

The Condensed-phase Optimized Molecular Potentials for Atomistic Simulation Studies (COMPASS) ab initio forcefield was used for all these applications. The simulation was performed with an interval of 1 femtosecond (fs) in each scenario, and the simulation steps were 2.0×10^5 with a cumulative dynamic time of 200.0 picoseconds (ps). In the meantime, atom configurations were saved as trajectory data in every 5000 frames in each case and dynamic. Figures 4–7 show the coating configuration of PTFE’s amorphous cell on Al_2O_3 (010) before and after MD simulation. Equation (1) was designed to model the interaction of covalent bonds between atoms and the interaction of van der Waals (vdW) in the wear-resistant layers [9]. Additionally, Equation (1) describes all bonded and non-bonded interactions in twelve forms. The first ten terms in Equation (1) are used to model cross-linked diagonals and off-diagonals, and the last two terms model non-bonded interactions (electrostatic (coulombic) and van der Waals). The first four terms reflect, in particular, the energies produced by the bonds stretching (b), bonds bending (θ), bond torsion (φ), and Wilson out-of-plane (χ) internal coordinates. The cross-coupling terms include combinations of two or three internal coordinates $[[b, \theta], [b, \varphi], [\theta, \varphi], [\theta, \theta, \varphi]]$ respectively.

$$\begin{aligned}
 E_{total} = & \sum_b [k_2 (b - b_o)^2 + k_3 (b - b_o)^3 + k_4 (b - b_o)^4] \\
 & + \sum_{\theta} [k_2 (\theta - \theta_o)^2 + k_3 (\theta - \theta_o)^3 + k_4 (\theta - \theta_o)^4] \\
 & + \sum_{\varphi} [k_1 (1 - \cos \varphi)^2 + k_2 (1 - \cos 2\varphi) + k_3 (1 - \cos 3\varphi)] \\
 & + \sum_{\chi} k_2 \chi^2 + \sum_{b, b'} k (b - b_o) (b' - b'_o) \\
 & + \sum_{b, \theta} k (b - b_o) (\theta - \theta_o) \\
 & + \sum_{b, \varphi} (b - b_o) [k_1 \cos \varphi + k_2 \cos 2\varphi + k_3 \cos 3\varphi] \\
 & + \sum_{\theta, \varphi} (\theta - \theta_o) [k_1 \cos \varphi + k_2 \cos 2\varphi + k_3 \cos 3\varphi] \\
 & + \sum_{b, \theta} k (\theta' - \theta'_o) (\theta - \theta_o) \\
 & + \sum_{\theta, \theta, \varphi} k (\theta - \theta_o) (\theta' - \theta'_o) \cos \varphi + \sum_{ij} \frac{q_i q_j}{r_{ij}} \\
 & + \sum_{ij} \epsilon_{ij} [2 \left(\frac{r_{ij}^o}{r_{ij}} \right)^9 - 3 \left(\frac{r_{ij}^o}{r_{ij}} \right)^6]
 \end{aligned} \tag{1}$$

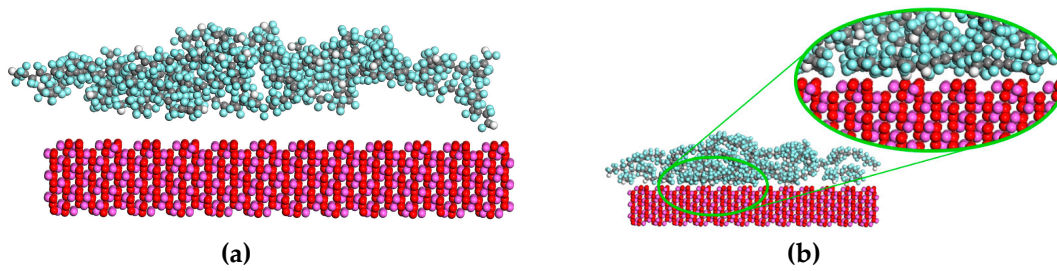


Figure 4. Coating of an amorphous cell of K10 chain length of PTFE on Al₂O₃ (010) (a) before MD simulation (b) after MD simulation.

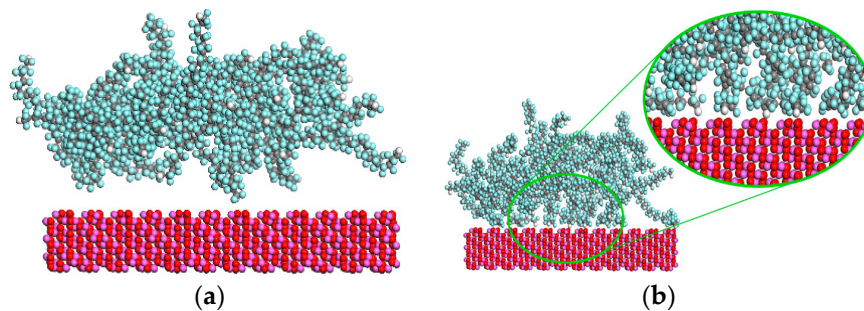


Figure 5. Coating of an amorphous cell of K20 chain length of PTFE on Al₂O₃ (010) (a) before MD simulation (b) after MD simulation.

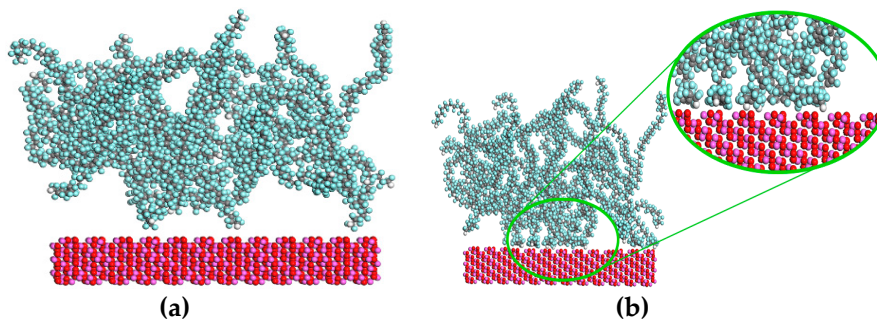


Figure 6. Coating of an amorphous cell of K30 chain length of PTFE on Al₂O₃ (010) (a) before MD simulation (b) after MD simulation.

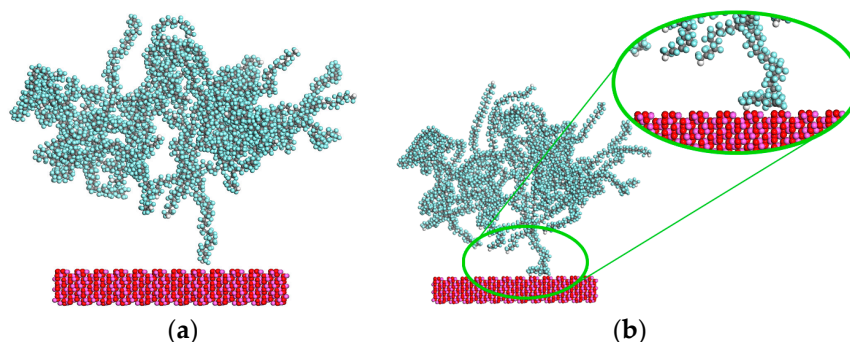


Figure 7. Coating of an amorphous cell of K40 chain length of PTFE on Al₂O₃ (010) (a) before MD simulation (b) after MD simulation.

The static mechanical properties of the equilibrated system of PTFE/Al₂O₃ (010) need to be calculated. The balance of temperature and energy (non-bond and potential) simultaneously determines the system's equilibrium, significantly, when energy and temperature fluctuate within a maximum

of $\pm 5\%$ – 10% [10]. The scenario is considered to reach the equilibrium state when the temperature is 298 K. The Forcite module in materials studio (MS) version 7.0 of Accelrys Inc. was used to implement all molecular dynamic calculations. Mechanical properties, cohesive energy density, and binding energy were calculated using the universal force field (UFF) based on the quantum mechanical method. The last eleven frames of the stable systems were determined. The stiffness matrix and flexibility matrix of the composite, shear modulus, and bulk modulus were determined using Reuss, Voigt, and Hill approximation [11]. The macro-level enhanced anti-erosive wear is close to the isotropic material, and comparable to isotropic materials.

The relationship between stress (σ) and strain (ϵ), with stiffness or elastic constants (C_{ij}) of the material, follows the generalized Hooke's law [12,13], as shown in Equation (2). Lamé constants, lambda (λ), and Mu (μ) describe the stress–strain relationships of isotropic material, as demonstrated in Equation (3). Meanwhile, Equation (4) is used to evaluate standard elastic parameters such as elastic modulus (E), bulk modulus (B), shear modulus (G), and Poisson ratio (ν). Further, the binding energy (E_b) is the mechanical (binding) energy required to disassemble a whole composite into separate parts. Equation (5) is used to quantify the binding energy where E_t is the single-point total energy of the equilibrated system after the interaction, E_p is the single point energy of the polymer, and E_s is the single point energy of the Al_2O_3 (010) surface before interaction with the polymer. The Hildebrand solubility parameter and cohesive energy density are defined in Equation (6) and calculated through the Forcite tool in each erosive wear-resistant composite of PTFE/ Al_2O_3 (010).

$$\begin{bmatrix} \sigma_1 \\ \sigma_2 \\ \sigma_3 \\ \sigma_4 \\ \sigma_5 \\ \sigma_6 \end{bmatrix} = \begin{bmatrix} C_{11} & C_{12} & C_{13} & C_{14} & C_{15} & C_{16} \\ C_{21} & C_{22} & C_{23} & C_{24} & C_{25} & C_{26} \\ C_{31} & C_{32} & C_{33} & C_{34} & C_{35} & C_{36} \\ C_{41} & C_{42} & C_{43} & C_{44} & C_{45} & C_{46} \\ C_{51} & C_{52} & C_{53} & C_{54} & C_{55} & C_{66} \\ C_{61} & C_{62} & C_{63} & C_{64} & C_{65} & C_{66} \end{bmatrix} \begin{bmatrix} \epsilon_1 \\ \epsilon_2 \\ \epsilon_3 \\ \epsilon_4 \\ \epsilon_5 \\ \epsilon_6 \end{bmatrix} \quad (2)$$

The below Equations (3)–(5) shows the stress–strain relations of Lamé constants and binding Energy

$$\lambda = \frac{1}{3}(C_{11} + C_{22} + C_{33}) - \frac{2}{3}(C_{44} + C_{55} + C_{66}), \quad \mu = \frac{1}{3}(C_{44} + C_{55} + C_{66}), \quad (3)$$

$$E = \mu \left(\frac{3\lambda + 2\mu}{\lambda + \mu} \right), \quad \nu = \frac{\lambda}{2(\lambda + \mu)}, \quad B = \lambda + \frac{2}{3}\mu, \quad G = \mu \quad (4)$$

$$E_b = E_t - (E_p + E_s), \quad (5)$$

3. Results and Discussion

The results obtained in the MD simulations and the elastic constants of each PTFE/ Al_2O_3 (010) are shown in Tables 2 and 3 below. In the case of the isotropic materials, Poisson's ratio ν may be expressed in terms of the bulk modulus B and the shear modulus G , which relate, respectively, to changes in size and shape. The Poisson ratio of all stable isotropic materials is found between numerical limits $\frac{1}{2}$ and -1 [14]. If the material were not isotropic, the Poisson ratio would be greater than one (see Figure 8). The plastic range is typically between 0.2 and 0.4; natural rubber is about 0.5 and thermoplastic starch (TPs) is between 0.1 and 0.4 [15]. Nevertheless, according to the polymer properties database in [16], the rubber Poisson ratio is never exactly 0.5; this means that the elastic bulk modulus would reach infinity, which is not possible. However, very close to $\frac{1}{2}$ values have been reported (0.4999) [16]. The composite attributed to K10 chain lengths of PTFE is typically a natural rubber, as seen in Figure 9e and Table 3. In comparison, the composite assigned to the chain length of K20 belongs to plastic or thermoplastic starch. The chain length of K30 shows the unstable isotropic, and the K40 chain length seems to possess the anisotropic range of Poisson's ratio, unstable by volume change but stable if constrained. The idea that the Milton map of bulk isothermal

modulus B versus shear module G , when $B/G \gg 1$ and $\nu \rightarrow 1/2$ (vertical axis) means materials such as rubber are extremely incompressible. This idea was discussed and clarified in [14] by Greaves et al. Bulk modulus's negative compressibility is usually forbidden in classical thermodynamics, but it could be possible due to a recent study [17]. A stable negative bulk modulus of material has been observed experimentally in the constrained form [18]. Structures can consist of bi-material components that can have negative properties, significantly negative compressibility (negative bulk modulus, i.e., increased size when the external pressure is increased and decreased size when external pressure diminishes) [17]. The degree of compression typically represents bond strengths and, thus, softer materials [19]. For this reason, the bulk modulus of the K10 chain length of PTFE/ Al_2O_3 (010) in Figure 9c exhibits the negative value, which demonstrates the resistance of the PTFE/ Al_2O_3 (010) composite to erosion and corrosion compared to other simulated arrangements of the PTFE/ Al_2O_3 (010) composite. This effect is strongly supported by the obtained calculated binding (mechanical) energy and bulk modulus of 6267.16 kJ/mol and -3709.54 GPa, respectively (see Figure 9c,d). The mass density, bulk modulus, and Young's modulus work in the same way to ensure their auto-correlation functionality is similar [20]. Mass density can also be related to the corrosion degree of the material in the sense that, if the surfaces corrode, oxidizing occurs and eventually creates rust, which takes up more room than the initial material. This expansion and reduced density can lead to a variety of defects, such as cracking [20]. The higher the density of the material, the closer the particles are squeezed into the material, and the denser the PTFE/ Al_2O_3 (010) composite is, which contributes to hardness [21]. Negative effective shear modulus depicts axisymmetrically deformed composites with opposite axisymmetric loading conditions [22].

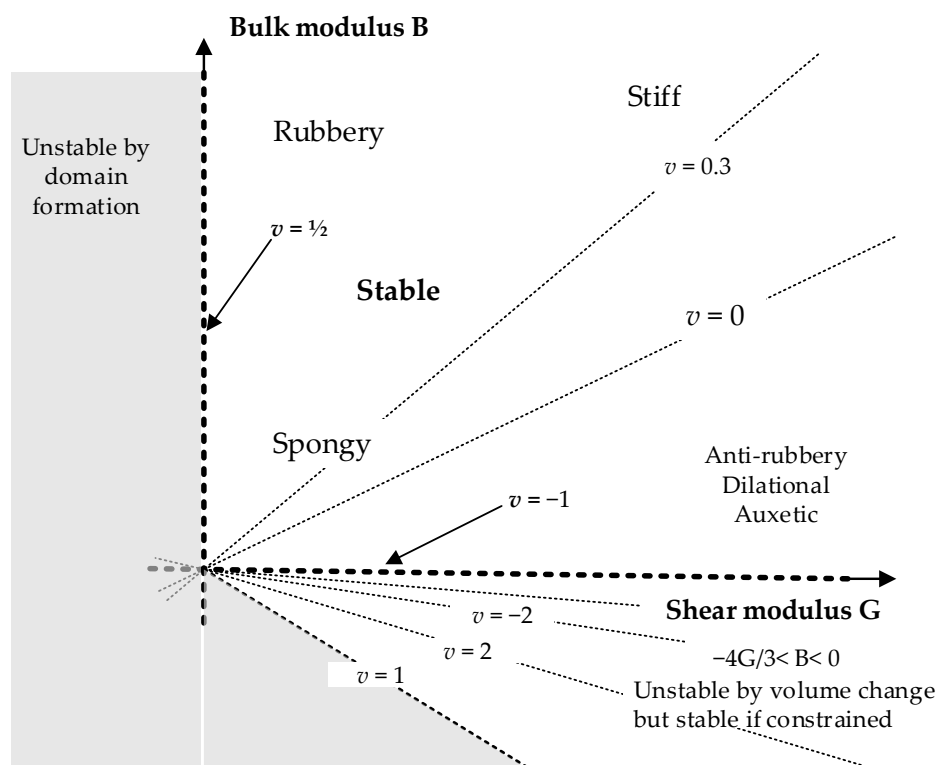


Figure 8. Milton map of bulk modulus versus shear modulus, showing the regimes of Poisson's ratio (ν) [14].

Table 2. The elastic stiffness matrix of PTFE/Al₂O₃ (010) composite.

Coating of an Amorphous Cell of K10 Chain Length of PTFE on Al ₂ O ₃ (010)						
C _{ij} (GPa)	1	2	3	4	5	6
1	-1276.94	-2274.16	-3758.69	-627.14	333.72	-253.96
2	-2274.16	-3386.35	-4816.39	-490.81	411.54	-323.10
3	-3758.69	-4816.39	-6567.59	-520.05	478.95	-328.83
4	-627.14	-490.81	-520.05	72.10	14.45	75.11
5	333.72	411.54	478.95	14.4466	-21.22	2.47
6	-253.96	-323.10	-328.83	75.11	2.47	-127.57
Coating of an Amorphous Cell of K20 Chain Length of PTFE on Al ₂ O ₃ (010)						
C _{ij} (GPa)	1	2	3	4	5	6
1	407.85	1468.53	-1695.44	2793.44	-587.12	1229.29
2	1468.54	2051.47	-81.20	2679.19	-532.33	851.38
3	-1695.44	-81.20	-4798.43	3515.44	-712.54	1884.61
4	2793.44	2679.19	3515.45	158.28	35.72	-171.47
5	-587.12	-532.33	-712.53	35.72	-29.93	-23.67
6	1229.29	851.38	1884.61	-171.47	-23.67	-422.33
Coating of an Amorphous Cell of K30 Chain Length of PTFE on Al ₂ O ₃ (010)						
C _{ij} (GPa)	1	2	3	4	5	6
1	6455.40	2093.16	368.40	-344.27	2804.84	-7985.71
2	2093.16	-2217.00	-4349.66	-15.84	2656.07	-7700.60
3	368.34	-4349.66	-9322.88	-122.49	3771.29	-9737.98
4	-344.27	-15.83	-122.49	-15.789	-34.00	414.38
5	2804.84	2656.07	3771.29	-34.009	-47.43	-144.01
6	-7985.71	-7700.60	-9737.98	414.38	-144.01	531.12
Coating of an Amorphous cell of K40 chain Length of PTFE on Al ₂ O ₃ (010)						
C _{ij} (GPa)	1	2	3	4	5	6
1	685.48	587.11	-111.84	-1777.92	892.86	-448.15
2	587.11	453.74	-440.53	-1917.85	969.05	-419.62
3	-111.84	-440.53	-1064.19	-1594.49	880.50	-540.85
4	-1777.92	-1917.85	-1594.49	131.19	-7.49	-61.23
5	892.86	969.05	880.50	-7.49	-90.60	81.79
6	-448.15	-419.62	-540.84	-61.23	81.79	102.39

Table 3. The binding energy and mechanical properties of the K (10, 20, 30 and 40) PTFE/Al₂O₃ (010) composites.

Property	K10 Chain Length	K20 Chain Length	K30 Chain Length	K40 Chain Length
Binding Energy, E_b (kJ/mol)	6267.16	4271.05	3428.92	590.58
Elastic Modulus, E (GPa)	-76.52	-279.89	481.04	243.28
Shear Modulus, G (GPa)	-25.56	-97.99	155.96	47.66
Bulk Modulus, B (GPa)	-3709.54	-649.04	-1902.78	-38.54
Poisson's Ratio, ν (GPa)	0.49	0.42	0.54	1.55

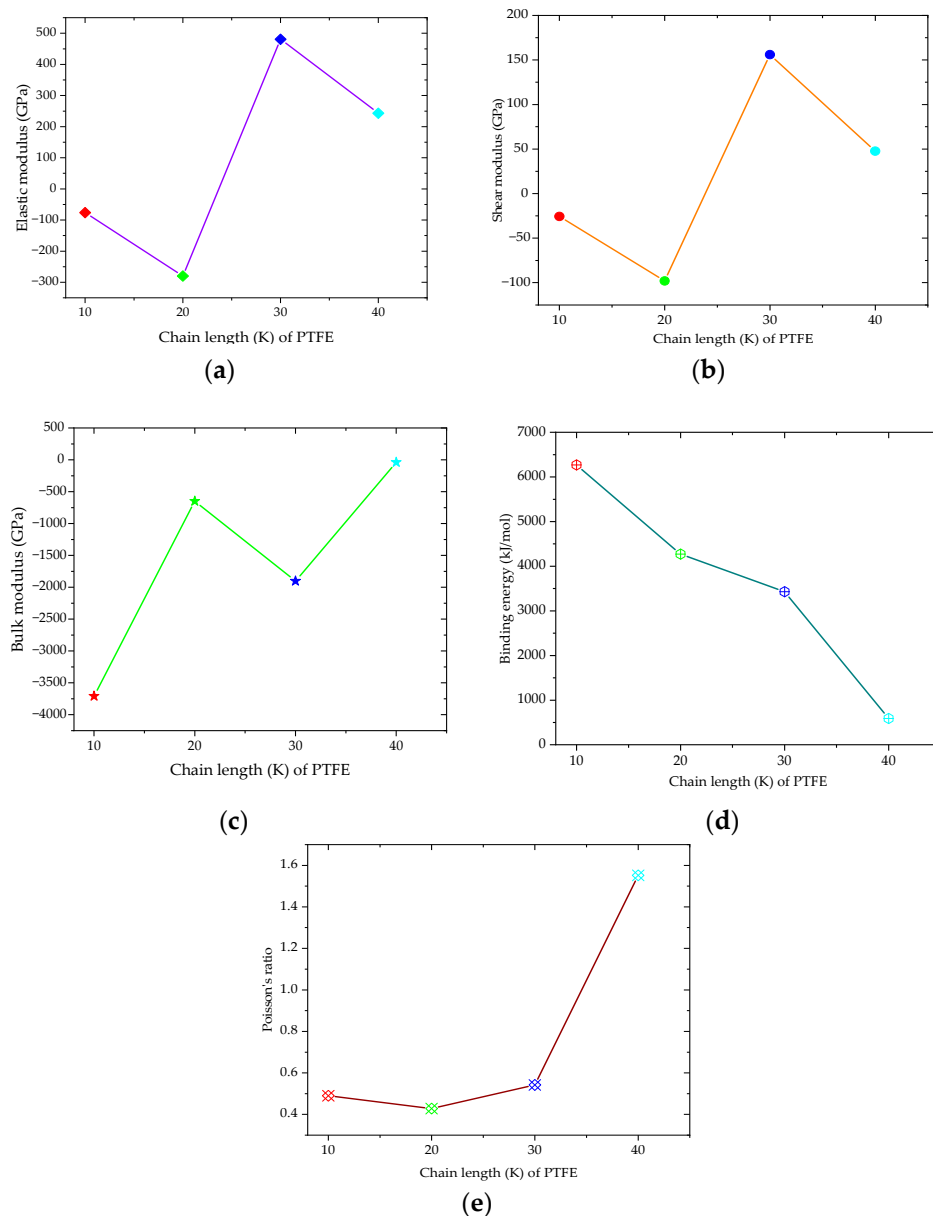


Figure 9. The plot of the calculated mechanical properties (a) elastic modulus, (b) shear modulus, (c) bulk modulus, (d) binding energy, and (e) Poisson's ratio against chain length (K) of PTFE.

It seems in Table 3 and Figure 9b that the K10 and K20 chain lengths of PTFE/Al₂O₃ (O10) show the negative shear modulus of -25.56 and -97.99 GPa, respectively. Combining their binding energies of 6267.16 and 4271.05 kJ/mol, respectively, forms the most desired strengths to overcome the surge imploding of pressure from the water cavity, causing water valves' erosion and corrosion. The estimated implosive pressure was of the order of 10^3 – 10^4 MPa and its period 2 – 3 μ s [23]. The simulated composite of K10 chain length exhibits stronger incompressibility of -3709.54 GPa and abundant binding energy of 6267.16 kJ/mol and unique moderate negative elastic and shear modulus (Figure 9a,b). Negative stiffness is possible in the systems, such as prestrained objects, including post-buckled elements, single-cell models, and post-buckled flexible tubes, containing stored energy [24,25]. The negative stiffness principle has been studied theoretically and experimentally in composite materials [25]. Stable negative structural stiffness is known, both theoretically and experimentally. The negative material stiffness, namely the bulk modulus (inverse compressibility) of a constrained solid elastic body of any dimension, is stable within the elasticity principle [18]. Double-negative metamaterials can be obtained by

combining negative effective mass and negative effective modulus [26]. Similar to electromagnetic (EM) metamaterials, the integration of resonant structures into blocks of an elastic metamaterial achieves negative successful elastic parameters [27]. Negative parameters, especially compressibility, will resist the compressive force generated by the microjets and prevent the material surface from undergoing plastic deformation (plastic flow), ultimately enhancing erosion and corrosion protective performance. According to Lee SH and Lee SB in [28], the Hildebrand solubility parameter (δ_H) is usually expressed as the square root for a chemical compound's cohesive energy density (CED), as Equation (6) depicts.

$$\delta_H = CED^{1/2} = (\Delta U/V)^{1/2} = [(\Delta H^{vap} - RT)/V]^{1/2} \quad (6)$$

where ΔU , ΔH^{vap} and V are internal molar energy, vaporization enthalpy (298 K), and molar volume, respectively. The solubility parameter (δ_H) has been widely used for predicting the solubility of various chemicals in organic solvents. Water as a polar solvent is likely to cause a hydrophobic effect in a valve chamber. The solubility parameter as a square root of cohesive energy density is a notable characteristic that distinguishes the nonpolar compound's hydrophobic nature. The higher value of the solubility or cohesive energy density of the nonpolar compound, the higher the hydrophobicity and bond strength, and the higher the corrosion protective performance. Molecules with stronger interactions have higher values of the cohesive energy density and solubility parameters, promoting the hydrophobic effect and improving the valve chamber's anti-corrosion and wear properties. In this work, it has been identified that solubility parameter (δ_H) and cohesive energy density values tended to decrease as the chain length increased (see Table 4). Based on Table 4, the wear-resistant coating of PTFE/ Al_2O_3 (010) with K10 chain length shows promising results for valve protection. These results can resist water hydraulic cavitation erosion and corrosion due to its higher cohesive energy density (CED) and solubility parameter of $(6.885 \pm 0.00076) \times 10^9$ J/m³ and (82.974 ± 0.005) (J/cm³)^{0.5}, respectively, compared to other simulated results of K (20, 30 and 40) of PTFE/ Al_2O_3 (010).

Table 4. The cohesive energy density (CED) and the Hildebrand solubility parameter of the K (10, 20, 30, and 40) PTFE/ Al_2O_3 (010) composites.

Chain Length (K)	CED (J/m ³) × 10 ⁹	Solubility Parameter (J/cm ³) ^{0.5}
10	6.885 ± 0.00076	82.974 ± 0.005
20	4.370 ± 0.00104	66.110 ± 0.008
30	2.691 ± 0.00077	51.876 ± 0.007
40	0.9 ± 0.00078	30.000 ± 0.013

4. Conclusions

The mechanical properties of the K10 and K20 chain lengths of PTFE/ Al_2O_3 (010) possess negative values of elastic modulus, shear modulus, and bulk modulus. In most elastic structures, we expect positive stiffness, such that the deformed material experiences force in the same direction as the deformation. Negative stiffness is possible in structures, such as prestrained objects and post-buckled components, that contain stored energy essential to rebound cavitation jet impacts. The same applies to bulk modulus; negative bulk modules are shown to be feasible in a prestrained lattice and other crystalline materials. Furthermore, the K10 chain length composition shows the higher value of binding energy and negative bulk modulus of 6267.16 kJ/mol and −3709.54 GPa, respectively. Likewise, the K10 chain length possesses a higher cohesive energy density and solubility parameter of $(6.885 \pm 0.00076) \times 10^9$ J/m³ and (82.974 ± 0.005) (J/cm³)^{0.5}, respectively, which provides the best characteristics for high bond strength and hydrophobic effects and hence improved corrosion and wear-resistance of the surface. To conclude, this work is helpful and can be instructive for material design in water hydraulics to alleviate erosion and corrosion. Further research in the future should investigate the behavior of PTFE coatings of other substrates, such as tungsten carbide (WC), boron carbide (B4C), etc.

Author Contributions: M.K.M. conducted the fundamental analysis and executed the entire procedure and wrote the article; H.X. advised on the analysis and reviewed the analytical results; H.W. checked, revised, and looked at the literature. All authors have read and agreed to the published version of the manuscript.

Funding: The Natural Science Foundation of China supported this work under grant 5187511, Natural Science Foundation of the Heilongjiang Province of China under grant F2016003, “Jinshan Talent” Zhenjiang Manufacture 2025 Leading Talent Project, “Jiangyan Planning” Project in Yangzhong City.

Conflicts of Interest: The authors declare no conflict of interest.

References

1. Micu, L.M.; Lazar, I.; Circiumaru, A.; Bordeasu, I.; Pirvulescu, L.D.; Hluscu, M. New results regarding cavitation behavior of polymers modified with anorganic substances coated on bronze surfaces. *Mater. Plast.* **2018**, *55*, 460–463. [CrossRef]
2. Zheng, H.-W.; Shu, X.-Y.; Li, Y.; Zhao, J.-P. Mechanical properties of Fe-based amorphous–crystalline composite: A molecular dynamics simulation and experimental study. *Rare Met.* **2018**. [CrossRef]
3. Xu, Y.; Wu, H.; Yang, J.; Liu, R.; Zhou, Z.; Hao, T.; Nie, Y. Molecular simulations of microscopic mechanism of the effects of chain length on stereocomplex formation in polymer blends. *Comput. Mater. Sci.* **2020**, *172*, 109297. [CrossRef]
4. Chen, B.; O’Mahony, J.A. Impact of glucose polymer chain length on heat and physical stability of milk protein-carbohydrate nutritional beverages. *Food Chem.* **2016**, *211*, 474–482. [CrossRef] [PubMed]
5. Zhao, J.; Lu, L.; Rabczuk, T. The tensile and shear failure behavior dependence on chain length and temperature in amorphous polymers. *Comput. Mater. Sci.* **2015**, *96*, 567–572. [CrossRef]
6. Pacuť, J.; Rams-Baron, M.; Chrzęszcz, B.; Jachowicz, R.; Paluch, M. Effect of polymer chain length on the physical stability of amorphous drug–polymer blends at ambient pressure. *Mol. Pharm.* **2018**, *15*, 2807–2815. [CrossRef] [PubMed]
7. Mlela, M.K.; Xu, H.; Sun, F.; Wang, H.; Madenge, G.D. Material analysis and molecular dynamics simulation for cavitation erosion and corrosion suppression in water hydraulic valves. *Materials* **2020**, *13*, 453. [CrossRef]
8. Li, H.; Bahuleyan, B.K.; Johnson, R.P.; Shchipunov, Y.A.; Suh, H.; Ha, C.-S.; Kim, I. Morphology-tunable architectures constructed by supramolecular assemblies of α -diimine compound: Fabrication and application as multifunctional host systems. *J. Mater. Chem.* **2011**, *21*, 17938–17945. [CrossRef]
9. Sun, H.; Jin, Z.; Yang, C.; Akkermans, R.L.C.; Robertson, S.H.; Spenley, N.A.; Miller, S.; Todd, S.M. COMPASS II: Extended coverage for polymer and drug-like molecule databases. *J. Mol. Model.* **2016**, *22*, 47. [CrossRef]
10. Wang, J.; Jin, S.; Chen, S.; Li, L.; Wang, D.; Lu, Z.; Wang, N.; Wang, J. Molecular dynamic simulations for FOX-7 and FOX-7 based PBXs. *J. Mol. Model.* **2018**, *24*, 145. [CrossRef]
11. Chung, D.H.; Buessem, W.R. The Voigt-Reuss-Hill (VRH) Approximation and the Elastic Moduli of Polycrystalline ZnO, TiO₂ (Rutile), and α -Al₂O₃. *J. Appl. Phys.* **1968**, *39*, 2777–2782. [CrossRef]
12. Hua, X.; Wang, L.; Yang, S.J.P. Molecular dynamics simulation of improving the physical properties of polytetrafluoroethylene cable insulation materials by boron nitride nanoparticle under moisture-temperature-electric fields conditions. *Polymers* **2019**, *11*, 971. [CrossRef] [PubMed]
13. Muhammad, I.D.; Awang, M.; Mamat, O.; Shaari, Z.B. First-principles calculations of the structural, mechanical and thermodynamics properties of cubic zirconia. *World J. Nano Sci. Eng.* **2014**, *4*, 97. [CrossRef]
14. Greaves, G.N.; Greer, A.L.; Lakes, R.S.; Rouxel, T. Poisson’s ratio and modern materials. *Nat. Mater.* **2011**, *10*, 823–837. [CrossRef]
15. Rosato, D.; Rosato, D. DESIGN PARAMETER. In *Plastics Engineered Product Design*; Elsevier Science: Amsterdam, The Netherlands, 2003; pp. 161–197.
16. Polymer Properties Database. Relationship between Moduli of Elasticity. 2020. Available online: <http://polymerdatabase.com/polymer%20physics/Moduli.html> (accessed on 2 July 2020).
17. Gatt, R.; Grima, J. Negative compressibility. *Phys. Status Solidi (RRL)-Rapid Res. Lett.* **2008**, *2*, 236–238. [CrossRef]
18. Lakes, R.; Wojciechowski, K.W. Negative compressibility, negative Poisson’s ratio, and stability. *Phys. Status Solidi (B)* **2008**, *245*, 545–551. [CrossRef]
19. Cairns, A.B.; Goodwin, A.L. Negative linear compressibility. *Phys. Chem. Chem. Phys.* **2015**, *17*, 20449–20465. [CrossRef]

20. Schuëller, G.I. *Computational Methods in Stochastic Dynamics*, 1st ed.; Springer: Dordrecht, The Netherlands, 2011.
21. Corrosionpedia. Mass Density. 2019. Available online: <https://www.corrosionpedia.com/definition/1562/mass-density> (accessed on 24 May 2020).
22. Zhou, X.; Hu, G. Analytic model of elastic metamaterials with local resonances. *Phys. Rev. B* **2009**, *79*, 195109. [[CrossRef](#)]
23. Karimi, A.; Martin, J.L. Cavitation erosion of materials. *Int. Met. Rev.* **1986**, *31*, 1–26. [[CrossRef](#)]
24. Wang, Y.; Lakes, R. Composites with inclusions of negative bulk modulus: Extreme damping and negative Poisson's ratio. *J. Compos. Mater.* **2005**, *39*. [[CrossRef](#)]
25. Moore, B.; Jaglinski, T.; Stone, D.S.; Lakes, R.S. Negative incremental bulk modulus in foams. *Philos. Mag. Lett.* **2006**, *86*, 651–659. [[CrossRef](#)]
26. Su, Y.C.; Sun, C.T. Design of double negativity elastic metamaterial. *Int. J. Smart Nano Mater.* **2015**, *6*, 1–12. [[CrossRef](#)]
27. Wu, Y.; Lai, Y.; Zhang, Z.-Q. Elastic metamaterials with simultaneously negative effective shear modulus and mass density. *Phys. Rev. Lett.* **2011**, *107*, 105506. [[CrossRef](#)] [[PubMed](#)]
28. Lee, S.H.; Lee, S.B. The Hildebrand solubility parameters, cohesive energy densities and internal energies of 1-alkyl-3-methylimidazolium-based room temperature ionic liquids. *Chem. Commun.* **2005**, *27*, 3469–3471. [[CrossRef](#)] [[PubMed](#)]

Publisher's Note: MDPI stays neutral with regard to jurisdictional claims in published maps and institutional affiliations.



© 2020 by the authors. Licensee MDPI, Basel, Switzerland. This article is an open access article distributed under the terms and conditions of the Creative Commons Attribution (CC BY) license (<http://creativecommons.org/licenses/by/4.0/>).